PCCP

Accepted Manuscript

ROYAL SOCIETY OF CHEMISTRY

www.rsc.org/pccp

Chemical Science

ARTICLE

The Transition Metal Surface Passivated Edges of Hexagonal Boron Nitride (h-BN) and the Mechanism of h-BN's Chemical Vapor Deposition (CVD) Growth

Received 00th January 20xx,
Accepted 00th January 20xx

DOI: 10.1039/x0xx00000x

www.rsc.org/

Ruiqi Zhao,[a,b,c] Feifei Li,[b] Zhirong Liu,[c] Zhongfan Liu,[c] and Feng Ding,[a,d]*

Edge structure and stability are crucial in determining both the morphology and the growth behaviours of hexagonal boron nitride (h-BN) domains in chemical vapour deposition (CVD) growth under the near thermal equilibrium condition. In this study, various edges of h-BN on three typical transition metal surfaces used for h-BN's CVD growth, Cu(111), Ni(111) and Rh(111), are explored with density functional theory calculations. Different from that in vacuum, our study presents that the formation of non-hexagonal rings, such as pentagon, heptagon or their pairs, are energetically not preferred and both zigzag (ZZ) edges are more stable than the armchair (AC) edge on all the explored catalyst surfaces under the typical condition of h-BN's CVD growth, which explains the broad experimental observation of triangular h-BN domains. More importantly, our results indicate that, instead of pristine ZZ edge terminated with nitrogen atoms (ZZN), the triangular BN domains observed in experiments are likely to be enclosed with ZZ Klein edges having dangling atoms, ZZB + N or ZZN + B. Composed with binary composition. By applying the theory of Wulff construction, we predicted that the equilibrium shape of a BN domain could be a hexagon enclosed with nitrogen-rich AC edges, triangles enclosed with two different types of ZZ Klein edges or a hexagon enclosed with boron-rich AC edges if the growth is under N-rich, neutral or B-rich environment, respectively. This study presents how the edges and equilibrium shapes of h-BN domains can be controlled during the CVD synthesis and provides a guideline for further exploring the growth behaviours and improving the quality of CVD-prepared h-BN films.

1. Introduction

The absence of a gap in graphene hinders its applications in many fields. For this reason, 2D semiconductors have recently emerged for their possible use in optoelectronics[1-3]. Among them, hexagonal boron nitride (h-BN) has attracted considerable attention. Besides its intrinsic high bandgap, h-BN can also introduce a gap in graphene and retain the high carrier mobility by forming intralayer hybrid structures with carbon atoms[4-9] or being used as atomic flat substrate[10-12]. A primary prerequisite of applications is to synthesize high quality h-BN in large scale. To this end, transition metal catalysed chemical vapor deposition (CVD) growth with borazine ($N_3B_3H_6$)[13,14] and ammonia borane (NH_3–BH_3)[15,16] as BN precursors is a promising approach. Single-layer h-BN has been synthesized on various transition metal surfaces, such as Cu(111),[17] Ni(111),[18] Ir(111),[19] Pt(111),[20-22] Rh(111),[13,14,23-25] Ru(0001)[26-29] and so on. However, the as-produced h-BN films usually suffer from many defects, such as voids and linear grain boundaries.[28] Therefore, understanding the mechanisms that govern the behaviour of h-BN growth on the transition metal surfaces at atomistic level is very important for further improving the quality of CVD synthesized h-BN samples.

The structures and stabilities of various edges are crucially important in determining the optimal shapes and the growth behaviours of 2D materials. Our previous study on the stabilities of free-standing h-BN edges in vacuum has shown that both the self-reconstructions and the chemical potential difference between B and N can greatly influence the edge structures and the stabilities.[30] Previously, it was reported that the transition metal passivation also contributes greatly to the structures and stabilities of the edges and can further influence the growth behaviours of CVD-grown graphene.[31,32] Similarly to the synthesis of graphene, various transition metal substrates are used as catalysts in the synthesis of h-BN. However, the role of metal substrates in the growth of h-BN, such as the influence on the edge structures and the growth kinetics, remains unexplored until now. Here, we studied the edge reconstructions and stabilities of h-BN on the (111)

[a] Beijing Computational Science Research Center, Beijing 100084, China. E-mail: feng.ding@polyu.edu.hk.
[b] School of Physics and Chemistry, Henan Polytechnic University, Henan 454003, China
[c] State Key Laboratory for Structural Chemistry of Unstable and Stable Species, Beijing National Laboratory for Molecular Sciences (BNLMS), and Center for Nanochemistry, College of Chemistry and Molecular Engineering, Peking University, Beijing 100871, China
[d] Institute of Textiles and Clothing, Hong Kong Polytechnic University, Kowloon, Hong Kong, ChinaAddress here.

† Electronic Supplementary Information (ESI) available: Tests of stable configurations, edge energies of free standing h-BN and h-BN on different metals, maganetism in some typical models, formation energies vs. orientations, Wulff shapes of h-BN on Cu(111), Ni(111) and Rh(111) at different chemical potential difference. See DOI: 10.1039/x0xx00000x

surface of three typical transition metals for h-BN CVD growth, Cu, Ni and Rh. Our study shows that the edge stabilities of h-BN are distinctly different from that in vacuum due to the strong interaction between the metal surface and the edge atoms of h-BN domains. Two types of ZZ Klein edges[33,34] with dangling atoms, namely ZZB + N and ZZN + B, are the most stable ones on all metal substrates considered. Besides, the stabilities of the edges, the equilibrium shapes of h-BN domains as a function of chemical potential difference in vacuum, with H-termination and on the three metal surfaces, are presented and compared with experimental observations. We further showed that the growth behaviours of an h-BN domain could be controlled by selecting catalyst surfaces or tuning the experimental conditions. This work reveals the vital roles of transition metals in the synthesis of high quality CVD-grown h-BN.

2. Computational details

In this work, spin–polarized density functional theory (DFT) calculations were performed to study the reconstructions and stabilities of metal surface passivated various edges of h-BN crystal. The projector–augmented–wave (PAW) pseudopotential[35,36] was used for the core–electron interactions and Perdew–Burke–Ernzerhof (PBE) type generalized gradient approximation (GGA) was adopted for exchange–correlation functional[37,38] as implemented in the Vienna Ab initio Simulation Package (VASP). The comparison with the resulted calculated by the Van der Waals (VDW) functional proved that the PBE calculation is reliable because the formation energy of the h-BN are mainly contributed by the chemical binding between the edge atom and the catalyst surface. And similar standard DFT schemes were used to solve problems like this.[31,32] The kinetic energy cutoff for the plane wave basis was set as 400 eV and the energy convergence criterion of 10^{-4} eV was adopted in all calculations. The distances between both edges of BN nanoribbon (BNNR) and two BNNRs in neighbouring unit cells were set to be greater than 10 Å to ensure their interaction is negligible.

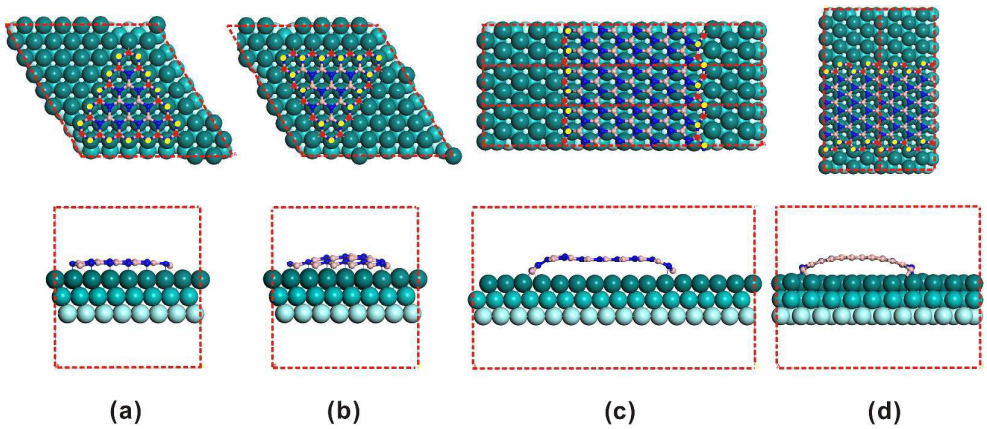

Fig. 1 Top and side views of relaxed models used to calculate the formation energies of different h-BN edges on transition metal surfaces: triangular h-BN flakes enclosed with pristine zigzag edges terminated with N atoms (namely ZZN) (a) and B atoms (namely ZZB) (b), (c) BNNR constructed with pristine ZZB edge (left) and reconstructed ZZN edge, ZZN57 (right), (d) BNNR constructed with pristine armchair (AC) edges. The boron and nitrogen atoms are shown in pink and blue (the atoms on the edges are highlighted in red and yellow), respectively. The metal atoms are shown from green to light green according to their depth from top to bottom. The red dashed rectangular boxes represent repeated unit cells adopted in DFT calculations.

Similar to graphene nanoribbons (GNRs), the edges of h-BN can be classified into zigzag (ZZ), armchair (AC) and chiral ones except that the zigzag edges can be further classified into ZZN (Fig. 1a) and ZZB (Fig. 1b) due to its binary composition.[30,39] The nomenclature of other reconstructed edges is in consistent with that used in our previous work.[30] The edge stabilities are measured by their formation energies, γ.[40] Metal-supported N- and B-terminated triangular h-BN flakes (see Fig. 1a and b) were used to calculate γ of pristine ZZN and ZZB edges and only Γ–point was considered in the DFT calculations due to the large unit cell size. BNNR models were used to calculate γ of reconstructed ZZ (Fig. 1c) and pristine/reconstructed AC (Fig. 1d) edges and the Monkhorst–Pack[41] grid sampling with different meshes was used to carry out the reciprocal space integrations. A three layered slab with the bottom layer fixed was used to mimic the bulk metals. Representative relaxed models seen from top and lateral are shown in Fig. 1. Here, Cu(111), Ni(111) and Rh(111) were selected because of their extensive applications in CVD growth of h-BN[13,17,18,23] and potential possibilities in obtaining high quality h-BN[42]. For Cu and Ni, the metal lattice is compressed or expanded to match that of h-BN due to the very small lattice mismatch [1.7% for Cu(111) and -0.84% for Ni(111)].[43] As reported in previous work, the current scheme is reliable.[31,43,44] For Rh, both expansion of h-BN and compression of Rh are implemented in order to reach a

compromise in lattice matching between BN and Rh(111) due to the relative significant lattice mismatch (6.7%).[13] For BN on Cu(111) and Ni(111), a supercell of 34.82 × 5.02 × 20 Å^3 (8.71 × 25.13 × 20 Å^3) with a k-point mesh of 1 × 7 × 1 (5 × 1 × 1) was used to calculate γ of reconstructed ZZ (pristine and reconstructed AC) edges. For h-BN on Rh(111), a supercell of 36.02 × 5. 20 × 20 Å^3 (9.00 × 26.00 × 20 Å^3) was used in all of the calculations. Nine (six) rows of zigzag (armchair) BNNRs with the middle three (two) rows fixed with a height of 3 Å to mimic infinite h-BN were put on metal surface.

There are three high symmetric sites on metal surfaces for B or N atoms, which produces six different structures of h-BN on a metal surface. The six configurations were studied carefully (see Part 1 and Fig. S1 in the electronic supplementary information, ESI) and the one with B adopting hcp position and N taking the top site was proved most stable and therefore was used in our simulations.

For pristine ZZN and ZZB, the formation energy of the edge is defined as:

$$\boldsymbol{\gamma_{ZZN}} = \frac{E_{BN\_M} - n_{BN}\mu_{BN} - n_N\mu_N - \mu_B - E_M}{3L} = \boldsymbol{\gamma^0_{ZZN}} - \frac{\Delta\mu}{3}, \quad (1)$$

$$\boldsymbol{\gamma_{ZZB}} = \frac{E_{BN\_M} - n_{BN}\mu_{BN} - n_B\mu_B - \mu_N - E_M}{3L} = \boldsymbol{\gamma^0_{ZZB}} + \frac{\Delta\mu}{3}, \quad (2)$$

For pristine AC edge, γ_{AC} can be defined as:

$$\boldsymbol{\gamma_{AC}} = \frac{E_{BN\_M} - n_{BN}\mu_{BN-E_M}}{2L}, \quad (3)$$

For reconstructed ZZ/AC edges, take ZZN57 as an example, γ_{ZZN57} is obtained by:

$$\boldsymbol{\gamma_{ZZN57}} = \frac{E_{BN\_M} - n_{BN}\mu_{BN} - E_M}{L} - \boldsymbol{\gamma_{ZZB}}, \quad (4)$$

In Eqs. (1)-(4), E_{BN_M} and E_M are the calculated energies of BN flakes/BNNRs on metal surface and the metal substrate, respectively; n_{BN} is the number of BN pairs, μ_{BN} is the energy of a BN pair in freestanding h-BN sheet, n_N (n_B) is the number of extra N(B) atoms in the triangular BN flakes, L is the length of the BN edge in the unit of nanometer, and the factor 2 or 3 accounts for the number of identical edges in each model considered, 2 for the BNNR models and 3 for the triangular domain models.

For the regular edges with orientation angles of - 30° (ZZN), 0° (AC) and 30° (ZZB), the formation energies can be directly calculated by using the models shown in Fig. 1 and Eqs. (1)-(4). For other edges composed with both AC and ZZ sites, their formation energies can be obtained by using the following analytical expression proposed by Liu et al. [40,45]

$$\boldsymbol{\gamma(\chi)} = |\boldsymbol{\gamma_0}|\boldsymbol{\cos(\chi + C)}, \quad (5\text{-}1)$$

where

$$|\boldsymbol{\gamma_0}| = \mathbf{2}\sqrt{\left(\boldsymbol{\gamma_{AC}}^2 + \boldsymbol{\gamma_{ZZX}}^2 - \sqrt{\mathbf{3}}\boldsymbol{\gamma_{AC}}\boldsymbol{\gamma_{ZZX}}\right)}, \quad (5\text{-}2)$$

$\gamma_{ZZX} = \gamma_{ZZB}$, $\boldsymbol{C} = \boldsymbol{arctan}\frac{\sqrt{3}\gamma_{AC} - 2\gamma_{ZZB}}{\gamma_{AC}}$, for $0° < \chi < 30°$, (5-3)

or

$\gamma_{ZZX} = \gamma_{ZZN}$, $\boldsymbol{C} = -\boldsymbol{arctan}\frac{\sqrt{3}\gamma_{AC} - 2\gamma_{ZZN}}{\gamma_{AC}}$, for $-30° < \chi < 0°$, (5-4)

Composed with binary composition, the edge stabilities can be further tuned by varying the chemical potential difference between B and N. Assuming that

$$\mu_{BN} = \mu_B + \mu_N, \quad (6)$$

the chemical potentials of B and N can be written as:

$$\mu_B = 0.5\mu_{BN} + \Delta\mu, \quad (7\text{-}1)$$

$$\mu_N = 0.5\mu_{BN} - \Delta\mu, \quad (7\text{-}2)$$

where $\Delta\mu$ is the chemical potential difference and is defined as $\Delta\mu = (\mu_B - \mu_N)/2$.[30,40] The edge formation energies, $\boldsymbol{\gamma^0_{ZZN}}$ and $\boldsymbol{\gamma^0_{ZZB}}$ in Eqs. (1) and (2) are obtained in case with $\Delta\mu = 0$. For edges with additional B/N atoms, $N*\Delta\mu$, where N is the number of additional atoms per unit length must be considered in the definition of the edge formation energy. More details about the energy expressions as functions of $\Delta\mu$ can be found in Table S1.

3. Results and discussion

Figure 1 shows the top and side views of the relaxed configurations of some typical atomic models used in our simulations. From the side views we can see that the edge atoms, especially the B atoms, tend to move towards the metal surface, indicating a strong binding between the edge atoms and underlying metal surface. In this study, we have explored twelve carefully designed edges. Their relaxed configurations are shown in Fig. 2.

In order to achieve an overall understanding on the effect of metal passivation, we plot the formation energies ($\Delta\mu = 0$) of some stable edges on metal surfaces in Fig. 3(a). For a comparison, the formation energies of the pristine edges and hydrogen terminated ones are also shown. More results including the formation energies and the relationship between the edge energies and the chemical potential difference between B and N, are summarized in Table S1.

From Fig. 3(a) we can see that, among the pristine edges, the AC edge is the most stable one followed by the ZZB + N and ZZN57 edges. While, if the edges are terminated with H atoms, the pristine ZZN edge becomes the most stable one followed with the ZZB + N and AC. Differently, once the edges are passivated by a metal surface, the Klein ZZ edge, ZZB + N becomes the most stable one on all of the three explored catalysts. Compared with the pristine edge, the formation energies of the ZZB + N edge is significantly lowered by 5.14 eV/nm (52%), 6.58 eV/nm (67%), and 7.56 eV/nm (77%) on Cu(111), Ni(111), and Rh(111) surfaces, respectively. Although the stabilities of the other two edges, ZZN and AC, highly depend on underlying metal surfaces(for example, the Cu(111) passivated ZZN edge is more stable than the AC edge, while they are nearly equal if passivated by Ni(111) and Rh(111)), they are also much lower than the pristine ones. In all cases, the formation energy of a metal surface passivated edge is always significantly lower than that of corresponding pristine one. And a similar reduction in formation energies for other types of edges can be found as well (see Table S1). In a

word, all the edge stabilities of h-BN can be remarkably improved by the passivation of underlying metal surfaces.

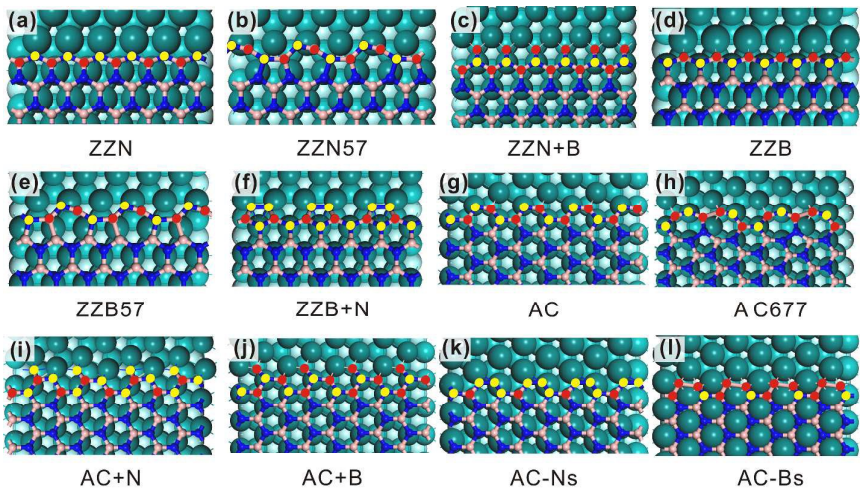

Fig. 2 Some of the low energy optimized edge structures of h-BN on the Ni(111) surface (same colour code has been used in Fig. 1).

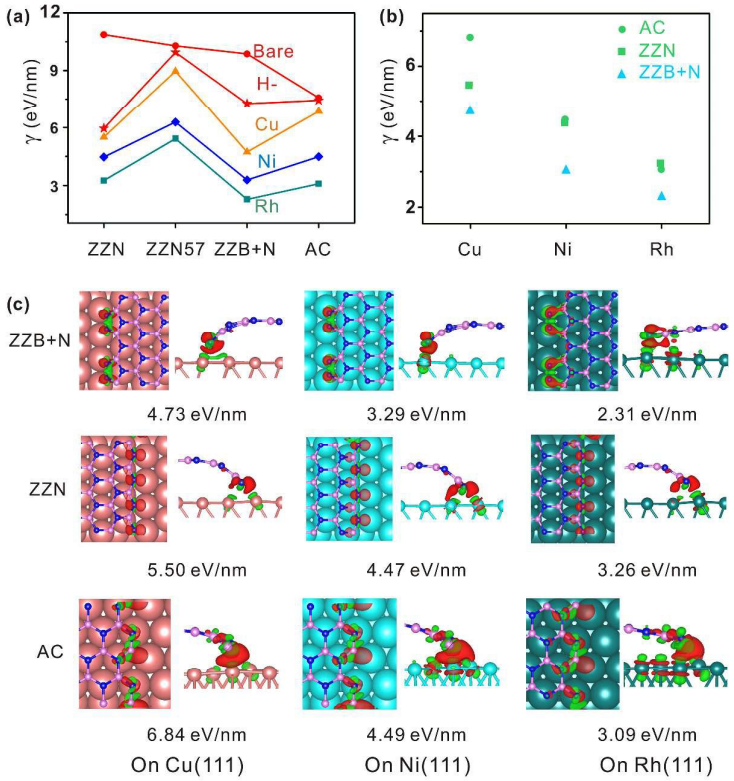

Fig. 3 (a) Formation energies (γ) of the edges of free-standing h-BN (both bare and H-terminated ones are included) and h-BN on the (111) surfaces of Cu, Ni and Rh, respectively. (b) Formation energies (γ) of ZZB + N, ZZN, and AC edges of h-BN on (111) surfaces of corresponding metals. (c) Charge difference distributions between BNNRs and underlying metals (only the parts with ZZB + N, ZZN and AC edges are shown here, the isosurface is 0.006 e/Å^3, the edge energies are also listed), in which red and green zones indicate gain and loss of charge, respectively. The formation energies are obtained with $\Delta\mu$ = 0. The lines in (a) serve as guides to the eye.

The extraordinary stability of pristine bare AC edge of h-BN is attributed to the formation of triple bonds between the outermost edge atoms.[30] To achieve a deep insight into the effect of metal surface passivation on the stabilities of various h-BN edges, we calculated the difference charge distributions between BNNRs and underlying metal surfaces. The results of

the ZZB + N, ZZN and AC edges on three metal surfaces are shown in Fig. 3c. From Fig. 3c we can see that all edges bend towards the metal surfaces and an obvious charge transfer occurs between the edge atoms and underlying metal surfaces. Take the edge ZZB + N as an example, for h-BN on Rh(111), the charge transfer occurs not only on the edge atoms but also on the bulk atoms of h-BN, which leads to a flat edge on the Rh(111) surface and an effective edge passivation. While, for h-BN on Cu(111) and Ni(111), the charge transfer is highly localized between the edge atoms and underlying metals, which leads to a highly curved edge towards the metal surface. Because of the higher activity of Ni than Cu, the edge formation energy of h-BN on Ni(111) surface is significantly lower than that on Cu(111) surface, which is similar as that of graphene on Ni(111) and Cu(111).[31,32] Similar stability variations can be found in the edges of ZZN and AC. Compared with Cu(111) and Ni(111), the edges passivated by the Rh(111) surface have even lower formation energy, which indicates that the activities of the three catalyst surfaces follows the order of Cu(111) < Ni(111) < Rh(111). Besides the stabilization, the charge transfer/redistribution may also induce the formation of local magnetism on the metal surface atoms (as indicated by the magnetism variation shown in Table S2), which may be interesting and deserves more detailed study.

We ignored the elemental chemical potential difference between B and N, i.e. $\Delta\mu$ = 0, in above discussion. While, experimentally, due to the binary composition of h-BN, $\Delta\mu$ depends on the experimental conditions and can be easily tuned by varying temperature and/or partial pressure of boron and nitrogen. To include the effect of experimental environment, we plotted the formation energies of each type of edges and the lowest ones as functions of $\Delta\mu$ in Fig. 4. From Fig. 4, we can see that:

(i) The pristine ZZN appears as the most stable one only in a narrow range of $\Delta\mu$ for h-BN on Cu(111) surface while disappears on Ni(111) and Rh(111);

(ii) On all explored catalyst surfaces, ZZB + N or ZZN + B is the most stable one in a large range of $\Delta\mu$, especially in the vicinity of $\Delta\mu$ = 0.

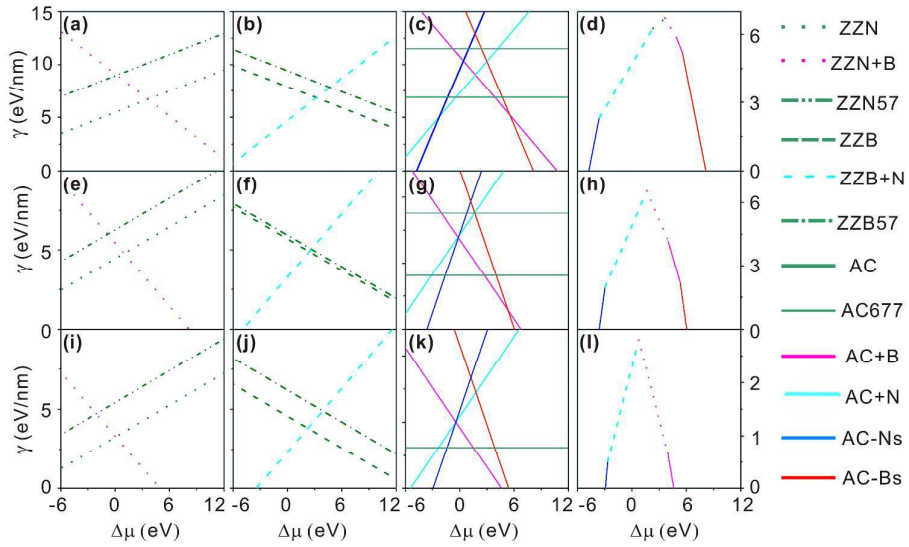

Fig. 4 Formation energies, γ and the lowest γ of edges as functions of the chemical potential difference (Δμ) between B and N for h-BN on Cu(111) (a-d), Ni(111) (e-h) and Rh(111) (i-l), respectively. The edges represented by different types of lines are also listed.

It should be noted that the most used precursors for h-BN CVD synthesis are borazine ($N_3B_3H_6$) and ammonia borane (NH_3–BH_3). This indicates that the supplies of B and N are at very similar amount and therefore Δμ can be determined accordingly. To further verify this, we consider the cases with B and N are supplied from the bulk and atomic phases. The energies of molecular N_2 (-8.30 eV/atom) and α-boron[46] (-6.67 eV/atom) are used as bulk references and the energies of atomic N (-3.11 eV/atom) and B (-0.27 eV/atom) are used as references of atomic phases. Therefore, the values of $\Delta\mu$ fall in the range of

$$0.815 \text{ eV} < \Delta\mu < 1.42 \text{ eV}, \quad (8)$$

Near the chemical range indicated by Eq. (8), we can see that ZZB + N is the most stable edge on Cu(111) and Ni(111) while on Rh(111), ZZN + B appears the stable one (see Fig. 4d, h and l). Besides that, ZZN is another candidate in a narrow range of chemical potential difference on Cu(111) surface.

The results discussed above are energies for edges at specific orientations and with high symmetries, i.e. AC, ZZ. It is impractical to obtain the formation energies of the low symmetric edges from direct DFT calculation because of the very large unit cell size, so we use the analytical expression in Eq. (5)[30,40] to obtain the formation energies of those tilted edges. The polar plots of formation energies (including h-BN on Cu111, Ni111 and Rh111) versus the orientation angles are

shown in Fig. S2. With the polar plots, we can easily construct the equilibrium shapes of h-BN domains by applying the Wulff's theorem.[47] The dashed lines in Fig. S2 shows the equilibrium shapes of h-BN domains on corresponding metal surfaces at different $\Delta\mu$. From Fig. S2, we can see that the shapes can be tuned by designing appropriate experimental conditions, such as selecting appropriate metals or tuning the ratio of B to N. Here, to show the important influence of H-termination and metal substrates on the equilibrium shapes clearly, we show the shape evolutions of h-BN domains as functions of $\Delta\mu$ in Fig. 5. From Fig. 5, we can see that when $\Delta\mu$ falls in the range of [0.815 eV, 1.42 eV](corresponds to the dark shaded area), the equilibrium shapes of pristine h-BN and the H-terminated ones are hexagonal and triangular enclosed with bare AC and H-terminated ZZN, respectively. Differently, in that specific range, the h-BN domains on all of the three metal surfaces are triangles---on Cu(111) and Ni(111), the triangles are enclosed with ZZB + N edges, while enclosed with ZZN + B edges on Rh(111), indicating the possibility of tuning edge types by designing metal catalysts.

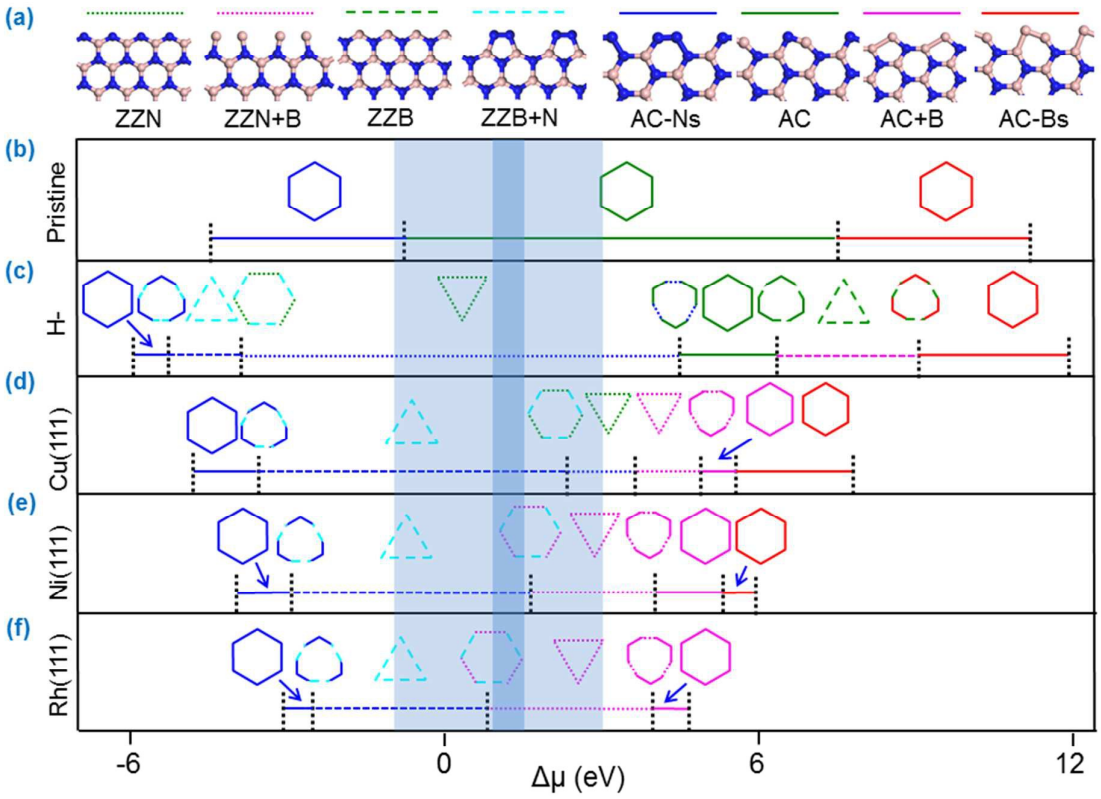

Fig. 5 The equilibrium shapes and edge structures of various h-BN domains: (b) the pristine ones, (c) the hydrogen-terminated ones and (d-f) the metal surface passivated ones, versus the chemical potential difference, $\Delta\mu$. The edges represented by different lines are shown in (a) and the dark shaded and shaded area corresponds to the range of $\Delta\mu$ indicated by Eqs. (8) and (9).

While, in real experiments, it is not difficult to change $\Delta\mu$ by 1 or 2 eV by varying growth conditions, such as by changing the partial pressures of BH_3 or NH_3. Thus a more practical range of $\Delta\mu$ in real experiments is:

$$-1 \text{ eV} < \Delta\mu < 3 \text{ eV}. \quad (9)$$

In that range, the equilibrium shapes of h-BN domains on metal surfaces may undergo a change from ZZB + N edged triangle to a ZZN + B or ZZN edged triangle and the hexagonal h-BN domains enclosed with two different types of ZZ edges may also be observed (the shaded area in Fig. 5). It is worthy of pointing out that ZZB + N/ZZN + B is the stable one in a quite wide range of $\Delta\mu$. This indicates that, instead of pristine ZZN, the experimentally observed triangular BN domains are very possible to be enclosed by the ZZB + N or the ZZN + B edges as observed experimentally.[28]

It is very interesting to address that the growth behaviour of h-BN on catalyst surface must be very different from that of pristine h-BN, where the AC edge is the most stable one or graphene, where the ZZ edge are proved to be the most stable one.[31] Both the dominating edges, ZZN + B and ZZB + N are terminated with a dangling atom on each unit cell as observed experimentally. The edge structures certainly will also change the growth kinetics of h-BN as well. The growth kinetics of h-BN domains terminated with ZZN + B/ZZB + N and ZZB/ZZN are shown in Fig. 6. For the ZZN or ZZB edge (Fig. 6f-j), forming a complete new ZZ atomic chain requires two independent steps—(i) the formation of a hexagon by adding three atoms,

2N + 1B/1N + 2B and (ii) the repeatable addition of a BN unit to form new hexagons on both shoulders of the 1D nucleus. Differently, each step of the growth of ZZB + N/ZZN + B (Fig. 6a-e) requires the addition of a BN unit only. Such a process should be able to greatly lower the energy required to initiate a 1D nucleus on the ZZB + N/ZZN + B edge and greatly increase the growth rate of h-BN. Besides, it should be noted that the BN edges with dangling atoms have been broadly observed experimentally.[28]

As discussed above, the most possible edges observed in experiments are ZZB + N or ZZN + B. The edge stabilities of h-BN on metals provide very useful information in controlling the CVD growth of h-BN:

i) The metal catalysts can greatly improve the stabilities of h-BN edges and thus should be able to lower the nucleation barrier of BN on catalyst surface as well;

ii) The stable edge, no matter ZZB + N or ZZN + B, contains no non-hexagon rings. This makes the self-healing of topological defects during the addition of B or N atoms to the edges unnecessary and ensures the high quality of the CVD synthesized h-BN.

iii) The relative stabilities of the edges can be controlled by designing experimental schemes carefully, such as selecting appropriate metal surface as catalysts, experimental temperatures and partial pressure of B or N in feedstock. This will also lead to the shape control of h-BN domains.

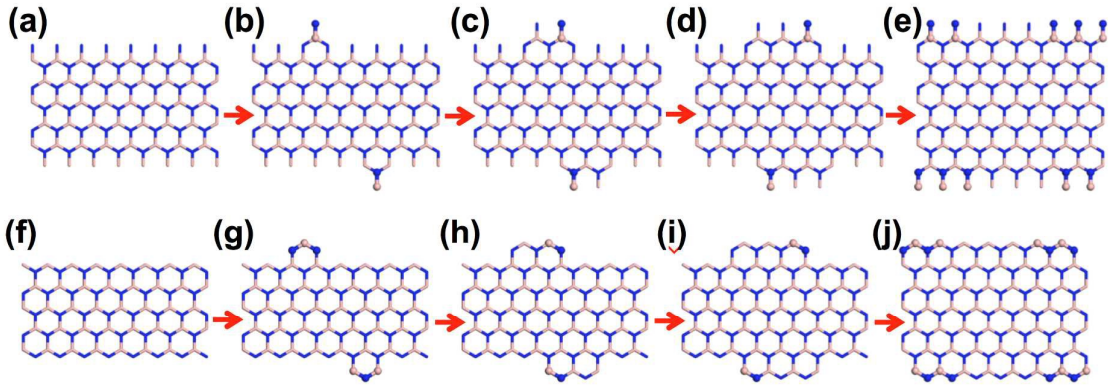

Fig. 6 The growth kinetics of the ZZN + B and ZZB + N edges in comparison with that of original ZZB and ZZN edges. Top panels (a-e) present the growth of another atomic chain on the ZZN + B (the lower one) edge and the ZZB + N edge (the upper one), where addition of a BN unit is required for each repeatable step of growth. Bottom panels (f-j) present the growth of ZZN (the lower one) and ZZB (the upper one) edges, where the formation of a complete hexagon by addition of 2B + 1N or 1B +2N is required to initiate the growth and the subsequent addition of a BN unit is required for each repeatable step of growth.

4. Conclusions

In summary, we have studied the structures and stabilities of various h-BN edges on metal surfaces with density functional theory calculations. And the behaviours of h-BN domains' CVD growth are revealed as well. Our results present that the metal surface passivation can remarkably lower the formation energies of the h-BN edges and change the types of stable edges. Furthermore, by varying the chemical potential difference between B and N, the near equilibrium domain shapes can be tuned from hexagonal to triangular enclosed with different types of edges. Besides, in agreement with experimental observations, our study also showed that the observed triangular BN flakes are mostly enclosed with ZZB + N or ZZN + B edges, which remarkably reduces the growth kinetics and efficiently prevents the formation of topological defects during CVD growth process. Overall, this study leads to a deep understanding on the metal surface passivation and growth mechanism of CVD-prepared h-BN.

Acknowledgements

R. Zhao was supported by the Natural Science Foundation of China (No. 21303041) and Beijing National Laboratory for Molecular Sciences (No. 2013006). Z.R. Liu was supported by NSFC (No. 21373015). R. Zhao thanks the support of high−performance grid computing platform of Henan Polytechnic University.

Notes and references

1 S. R. Tamalampudi, Y. Lu, R. Kumar U, R. Sankar, C. Liao, K. Moorthy B., C. Cheng, F. Chou, Y. Chen, *Nano Lett.* 2014, **14**, 2800-2806.

2 L. Viti, J. Hu, D. Coquillat, W. Knap, A. Tredicucci, A. Politano, M. S. Vitiello, *Adv. Mater.* 2015, doi:10.1002/adma.201502052.

3 H. Wang, L. Yu, Y. Lee, Y. Shi, A. Hsu, M. L. Chin, L. Li, M. Dubey, J. Kong,T. Palacios, *Nano Lett.* 2012, **12**, 4674-4680.

4 L. Ci, L. Song, C. H. Jin, D. Jariwala, D. X. Wu, Y. J. Li, A. Srivastava, Z. F. Wang, K. Storr, L. Balicas, F. Liu, P. M. Ajayan, *Nat. Mater.* 2010, **9**, 430-435.

5 Y. Gao, Y. Zhang, P. Chen, Y. Li, M. Liu, T. Gao, D. Ma, Y. Chen, Z. Cheng, X. Qiu, W. Duan, Z. Liu, *Nano Lett.* 2013, **13**, 3439-3443.

6 P. Sutter, R. Cortes, J. Lahiri, E. Sutter, *Nano Lett.* 2012, **12**, 4869-4874.

7 R. Y. Tay, M. H. Griep, G. Mallick, S. H. Tsang, R. S. Singh, T. Tumlin, E. H. T. Teo, S. P. Karna, *Nano Lett.* 2014, **14**, 839-846.
8 R. Zhao, J. Wang, M. Yang, Z. Liu, Z. Liu, *J. Phys. Chem. C* 2012, **116**, 21098-21103
9 J. Wang, R. Zhao, Z. Liu, Z. Liu, *Small*, 2013, **9**, 1373-1378.
10 R. Decker, Y. Wang, V. W. Brar, W. Regan, H.-Z. Tsai, Q. Wu, W. Gannett, A. Zettl, M. F. Crommie, *Nano Lett.* 2011, **11**, 2291-2295.
11 J. Xue, J. Sanchez-Yamagishi, D. Bulmash, P. Jacquod, A. Deshpande, K. Watanabe, T. Taniguchi, P. Jarillo-Herrero, B. J. LeRoy, *Nat. Mater.* 2011, **10**, 282-285.
12 L. Britnell, R. V. Gorbachev, R. Jalil, B. D. Belle, F. Schedin, M. I. Katsnelson, L. Eaves, S. V. Morozov, A. S. Mayorov, N. M. R. Peres, A. H. Castro Neto, J. Leist, A. K. Geim, L. A. Ponomarenko, K. S. Novoselov, *Nano Lett.* 2012, **12**, 1707-1710.
13 M. Corso, W. Auwärter, M. Muntwiler, A. Tamai, T. Greber, J. Osterwalder, *Science* 200 4, **303**, 217-220.
14 S. Berner, M. Corso, R. Widmer, O. Groening, R. Laskowski, P. Blaha, K. Schwarz, A. Goriachko, H. Over, S. Gsell, M. Schreck, H. Sachdev, T. Greber, J. Osterwalder, *Angew. Chem. Inter. Ed.* 2007, **46**, 5115-5119.
15 K. K. Kim, A. Hsu, X. T. Jia, S. M. Kim, Y. S. Shi, M. Hofmann, D. Nezich, J. F. Rodriguez-Nieva, M. Dresselhaus, T. Palacios, J. Kong, *Nano Lett.* 2012, **12**, 161-166.
16 G. Kim, A. R. Jang, H. Y. Jeong, Z. Lee, D. J. Kang, H. S. Shin, *Nano Lett.* 2013, **13**, 1834-1839.
17 S. Joshi, D. Ecija, R. Koitz, M. Iannuzzi, A. P. Seitsonen, J. Hutter, H. Sachdev, S. Vijayaraghavan, F. Bischoff, K. Seufert, J. V. Barth, W. Auwarter, *Nano Lett.* 2012, **12**, 5821-5828.
18 W. Auwärter, H. U. Suter, H. Sachdev, T. Greber, *Chem. Mater.* 2003, **16**, 343-345.
19 F. Orlando, R. Larciprete, P. Lacovig, I. Boscarato, A. Baraldi, S. Lizzit, S. T *J. Phys. Chem. C* 2011, 116, 157-164.
20 R. Laskowski, P. Blaha, Phys.l Rev. B 2010, 81, 075418.
21 E. Ćavar, R. Westerström, A. Mikkelsen, E. Lundgren, A. S. Vinogradov, M. L. Ng, A. B. Preobrajenski, A. A. Zakharov, N. Mårtensson, *Surf. Sci.* 2008, **602**, 1722-1726.
22 A. B. Preobrajenski, A. S. Vinogradov,M. L. Ng, E. Ćavar, R. Westerström, A. Mikkelsen, E. Lundgren, N. Mårtensson, *Phys. Rev. B* 2007, **75**, 245412.
23 G. Dong, E. B. Fourré, F. C. Tabak, J. W. M. Frenken, *Phys. Rev. Lett.* 2010, **104**, 096102.
24 F. Müller, S. Hüfner, H. Sachdev, *Surf. Sci.* 2009, **603**, 425-432.
25 R. Laskowski, P. Blaha, T. Gallauner, K. Schwarz, *Phys. Rev. Lett.* 2007, **98**, 106802.
26 A. Goriachko, Y. B. He, M. Knapp, H. Over, M. Corso, T. Brugger, S. Berner, J. Osterwalder, T. Greber, T. *Langmuir* 2007, **23**, 2928-2931.
27 P. Sutter, J. Lahiri, P. Albrecht, E. Sutter, *ACS Nano* 2011, **5**, 7303-7309.
28 J. Lu, P. S. E. Yeo, Y. Zheng, H. Xu, C. Gan, M. B. Sullivan, A. H. Castro Neto, K. P. Loh, *J. Am. Chem. Soc.* 2013, **135**, 2368-2373.
29 Y. Yang, Q. Fu, M. Wei, H. Bluhm, X. Bao, *Nano Res.* 2015, **8**, 227-237.
30 R. Zhao, J. Gao, Z. Liu, F. Ding, *Nanoscale* 2015, **7**, 9723-9730.
31 J. Gao, J. Zhao, F. Ding, *J. Am. Chem. Soc.* 2012, **134**, 6204-6209.
32 V. I. Artyukhov, Y. Liu, B. I. Yakobson, *Proc. Natl. Acad. Sci.* 2012, **109**, 15136-15140
33 D. J. Klein, *Chem. Phys. Lett.* 1994, **217**, 261-265.
34 P. Wagner, V. V. Ivanovskaya, M. Melle-Franco, B. Humbert, J.-J. Adjizian, P. R. Briddon, C. P. Ewels, *Phys. Rev. B* 2013, **88**, 094106.
35 G. Kresse, J. Furthmüller, *Comp. Mater. Sci.* 1996, **6**, 15-50.
36 G. Kresse, D. Joubert, *Phys. Rev. B* 1999, **59**, 1758.
37 J. P. Perdew, Y. Wang, *Phys.Rev. B* 1992, **45**, 13244.
38 J. P. Perdew, K. Burke, M. Ernzerhof, *Phys. Rev. Lett.* 1996, **77**, 3865.
39 P. Koskinen, S. Malola, H. Häkkinen, *Phys. Rev. Lett.* 2008, **101**, 115502.
40 Y. Liu, S. Bhowmick, B. I. Yakobson, *Nano Lett.* 2011, **11**, 3113-3116.
41 H. J. Monkhorst, J. D. Pack, *Phys. Rev. B* 1976, **13**, 5188.
42 R. Zhao, X. Zhao, Z. Liu, Z. Liu, F. Ding, The Orientation Control of h-BN on Transition Metal Surface during Chemical Vapor Deposition Growth, submitted.
43 P. A. Khomyakov, G. Giovannetti, P. C. Rusu, G. Brocks, J. van den Brink, P. J. Kelly, *Phys. Rev. B* 2009, **79**, 195425.
44 G. Giovannetti, P. A. Khomyakov, G. Brocks, V. M. Karpan, J. van den Brink, P. J. Kelly, *Phys. Rev. Lett.* 2008, **101**, 026803.
45 Y. Liu, A. Dobrinsky, B. Yakobson, *Phys. Rev. Lett.* 2010, **105**, 235502.
46 A. R. Oganov, J. Chen, C. Gatti, Y. Ma, Y. Ma, C. W. Glass, Z. Liu, T. Yu, O. O. Kurakevych, V. L. Solozhenko, *Nature* 2009, **457**, 863-867.
47 H. Conyers, *Phys. Rev. B* 1951, **82**, 87.